

PAPER • OPEN ACCESS

Kinesin-propelled label-free microtubules imaged with interference reflection microscopy

To cite this article: Gadiel Saper and Henry Hess 2020 New J. Phys. 22 095002

View the <u>article online</u> for updates and enhancements.

New Journal of Physics

The open access journal at the forefront of physics



Published in partnership with: Deutsche Physikalische Gesellschaft and the Institute of Physics



OPEN ACCESS

RECEIVED 13 May 2020

REVISED

31 July 2020

ACCEPTED FOR PUBLICATION 2 September 2020

DIIRLISHEN

17 September 2020

Original content from this work may be used under the terms of the Creative Commons Attribution 4.0 licence.

Any further distribution of this work must maintain attribution to the author(s) and the title of the work, journal citation and DOI.



PAPER

Kinesin-propelled label-free microtubules imaged with interference reflection microscopy

Gadiel Saper and Henry Hess*

Department of Biomedical Engineering, Columbia University, New York, NY, United States of America * Author to whom any correspondence should be addressed.

E-mail: hh2374@columbia.edu

Keywords: interference reflection microscopy, microtubules, kinesin, gliding assay

Supplementary material for this article is available online

Abstract

Interference reflection microscopy (IRM) utilizes the interference between the light reflected from the surface and the light reflected from an object to generate contrast and can be used to image nanometer size objects, such as a microtubule adhered to a surface as demonstrated by Mahamdeh *et al.* In *in vitro* gliding motility assays and in a variety of nanodevices, cytoskeletal filaments are propelled by surface-adhered motor proteins 20 to 50 nm above the surface. Here we employ IRM to image kinesin propelled label-free microtubules and show that these unlabeled microtubules are longer and move at higher velocities compared to rhodamine-labeled microtubules. IRM also provides information about the distance of an elevated microtubule from the surface and is used by us to follow microtubules crossover events. Finally, we perform the gliding assay without adding an oxygen scavenging system and show that there is significantly less photodamage for label-free microtubules measured with IRM compared to rhodamine-labeled microtubules imaged with fluorescence microscopy. This result suggests that IRM can be used for future experiments to further explore the effect of oxygen radicals on the gliding assay. Moreover, the increased velocity and length make label-free microtubules desirable for engineered devices based on molecular motors and filaments.

1. Introduction

Motor proteins and their associated filaments are extensively studied in engineering and biomedicine [1, 2]. A frequently used tool for these studies is the gliding motility assay, where surface-adhered motors (e.g. kinesins) propel filaments (e.g. microtubules) [3–6]. While the initial studies used differential interference contrast microscopy or darkfield microscopy to image the filaments [7–11], nowadays most gliding assays use filaments labeled with fluorophores and imaged with epi-fluorescence microscopy due to the high contrast ratio and the wide availability of suitable microscopes [12]. However, fluorescence microscopy has its own shortcomings: the intense excitation light can damage microtubules [13], cause cross-linking between filaments and motor proteins [14], and limit the observation time due to photobleaching [15], whereas the labeling of the filaments can potentially interfere with the movement of the motors along the filament [16]. Therefore, label-free methods of imaging continue to be explored [17–23].

Here, we apply a technique recently introduced by Mahamdeh *et al* [20] to the imaging of microtubules gliding on surface-adhered kinesins. Mahamdeh *et al* imaged label-free microtubules bound to the surface using interference reflection microscopy (IRM) to detect their polymerization kinetics. IRM generates contrast via the interference of light reflected by the coverslip surface and the object. It can be implemented—as Mahamdeh *et al* demonstrated—through a particularly simple alteration of the fluorescence microscope, that is the replacement of the filter cube consisting of excitation filter, beam splitter, and emission filter by a 50% beam splitter without wavelength selectivity (figure 1). We apply IRM to image label-free microtubules gliding on kinesin, contrast the observations with fluorescence imaging,

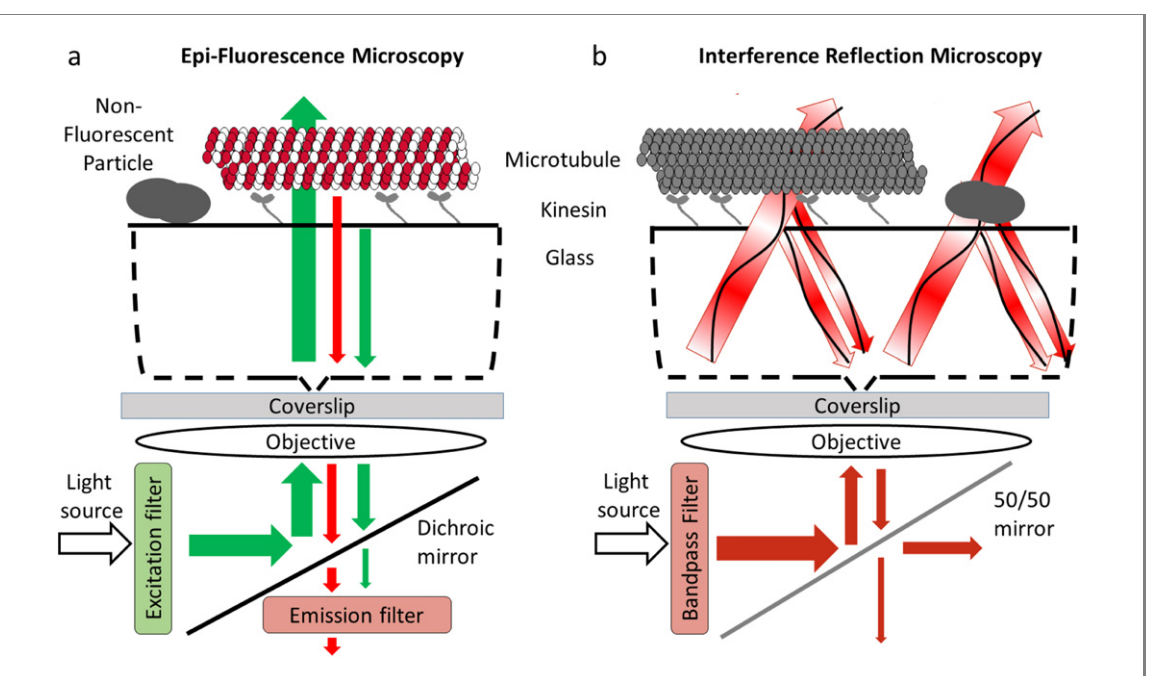


Figure 1. An illustration of the experimental set up. (a) Rhodamine-labeled microtubules can be imaged using fluorescence microscopy, which provides a signal from the labeled microtubules but not of any other non-fluorescent object on the surface. (b) For the IRM imaging of label-free microtubules, a filter cube without an emission filter and with a 50/50 mirror in place of the dichroic mirror is used. The excitation filter can be removed or replaced with a bandpass filter transmitting red light (590–650 nm) to reduce photodamage. Light reflected from objects on the surface with a refractive index higher than the solution (microtubules or other objects) is phase shifted by half a wavelength and interferes with light reflected from the interface between the coverslip and the solution. The destructive interference results in lower intensities, thus, the objects on the surface appear darker than their environment.

and demonstrate that IRM imaging avoids photodamage and generates information about nm-height changes while microtubule assembly and gliding benefit from the absence of interfering fluorophores.

2. Experimental section

2.1. Rhodamine-labelled microtubule preparation

Microtubules were polymerized from 20 μ g of lyophilized rhodamine-labelled tubulin (Cytoskeleton Inc., TL590M) in 6.25 μ l of polymerization buffer containing BRB80 buffer, with 4 mM MgCl₂, 1 mM GTP and 5% dimethylsulfoxide. BRB80 buffer is composed of 80 mM piperazine-N,N'-bis(2-ethanesulphonic acid), 1 mM MgCl₂ and 1 mM ethylene glycol tetraacetic acid (EGTA), adjusted to a pH of 6.89 with potassium hydroxide (KOH). The solution was incubated on ice for 5 min and then placed into a 37 °C water bath for 30 min. The polymerized microtubules were then diluted twenty-fold into BRB80 buffer containing 50 μ M paclitaxel.

2.2. Label-free microtubule preparation

Lyophilized tubulin (Cytoskeleton Inc., T240) was reconstituted with BRB80 buffer containing 4.7 mM MgCl₂, 1.2 mM GTP to a concentration of 3.7 mg ml⁻¹, divided into 5.4 μ l aliquots, and immediately flash frozen with liquid nitrogen and stored at $-80\,^{\circ}$ C. To polymerize the tubulin, an aliquot was thawed and 0.9 μ l dimethylsulfoxide was added to yield a total of 6.5 μ l polymerization buffer with 3.2 mg ml⁻¹ tubulin. The solution was incubated 5 min on ice and then for 30 min at 37 °C water bath. The polymerized microtubules were then diluted twenty-fold into BRB80 buffer containing 50 μ M paclitaxel.

2.3. Kinesin preparation

A kinesin construct consisting of the wild-type, full-length *Drosophila melanogaster* kinesin heavy chain and a C-terminal His tag [24] was expressed in *Escherichia coli*, purified using a Ni-NTA column, and flash frozen with liquid nitrogen in a buffer consisting of 40 mM imidazole, 300 mM NaCl, 0.76 g L⁻¹ EGTA, 37 mg L⁻¹ EDTA, 50 g L⁻¹ sucrose, 0.2 mM TCEP and 50 μ M Mg-ATP at pH 7 by the team of G. Bachand at the Center for Integrated Nanotechnologies (Sandia National Laboratory).

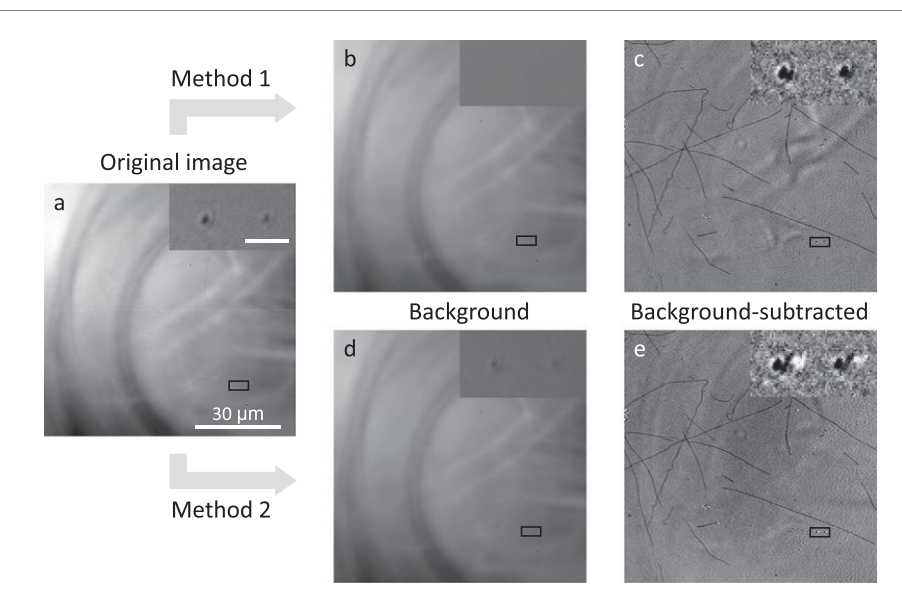


Figure 2. Interference reflection microscopy images of label-free microtubules before and after background subtraction. (a) Unedited IRM image of microtubules and other objects on the surface. Rings originate from uneven illumination due to structures in the excitation light path. An example of an immobile object on the surface is marked with a rectangular box and enlarged on the top right of the image (inset scale bar: 2 μ m). (b) Background computed by calculating the pixelwise median of 150 images taken as the stage is moved to a different location for each image. (c) Image after subtracting the background from (b) shows both microtubules and objects on the surface. (d) Background computed by calculating the pixelwise median of 433 images taken of the same location over time. (e) Image after subtracting the background from (d) shows the dark (low intensity) microtubules as well as distorted objects appearing due to stage-drift (inset).

2.4. Gliding assay

A top (22 mm \times 22 mm) and a bottom (60 mm \times 24 mm) coverslip were cleaned by washing twice with ethanol, twice with ultrapure water, sonicating for 5 min in ultrapure water and dried in an oven at 75 °C for 45 min. The coverslips were assembled into a flow cell using two double-sided adhesive tape strips. The flow cell was filled with BRB80 buffer containing 0.5 mg ml $^{-1}$ casein. After 5 min, the solution was exchanged for the kinesin motor solution containing BRB80 buffer with 0.5 mg ml $^{-1}$ casein, 1 mM ATP and kinesin twenty-fold diluted from the stock solution. The kinesin solution was exchanged after 5 min against the microtubule solution containing 0.004 mg ml $^{-1}$ tubulin, 0.5 mg ml $^{-1}$ casein, 10 μ M paclitaxel and 1 mM ATP in BRB80. In the fluorescence microscopy experiments, the microtubule solution also contained an enzymatic antifade system consisting of 20 mM D-glucose, 0.2 mg ml $^{-1}$ glucose oxidase, 8 μ g ml $^{-1}$ catalase and 10 mM dithiothreitol (unless otherwise noted). All experiments were performed at 23.5 \pm 2 °C.

2.5. Microscopy

The microtubules were imaged using a Nikon Eclipse Ti epifluorescence microscope equipped with a sCMOS camera (Zyla 4.2, Andor Inc.) and a 100×0 il objective (NA = 1.49). The sample was illuminated with an LED-based white light source (SOLA light engine, Lumencore Inc.). For the IRM, the light intensity was set to 51% of the maximum output and for the fluorescence images it was set to 8%. For the fluorescence imaging, an HQ R/DII filter cube (Nikon Inc.) was used. For the IRM, a filter cube with a 590–650 nm bandpass filter (ET620/60, Chroma Inc.) in the excitation filter position, and a 50/50 mirror (21 000, Chroma Inc.) in place of the dichroic mirror was used, while the aperture diaphragm was almost all the way closed and moved off-center to yield the best contrast. The camera exposure time was 100 ms for the IRM and 50 ms for the fluorescence microscopy measurements.

2.6. Analysis

The images were analyzed using Fiji ImageJ software and the data was analyzed with Fiji ImageJ and Matlab (MathWorks Inc.).

3. Results and discussion

3.1. IRM is used to measure kinesin propelled label-free microtubules

We followed the visual protocol of Mahamdeh *et al* [25] to image the microtubules with IRM. The utilization of the 50/50 mirror, a minimized diameter of the aperture diaphragm, as well as oblique

New J. Phys. 22 (2020) 095002 G Saper and H Hess

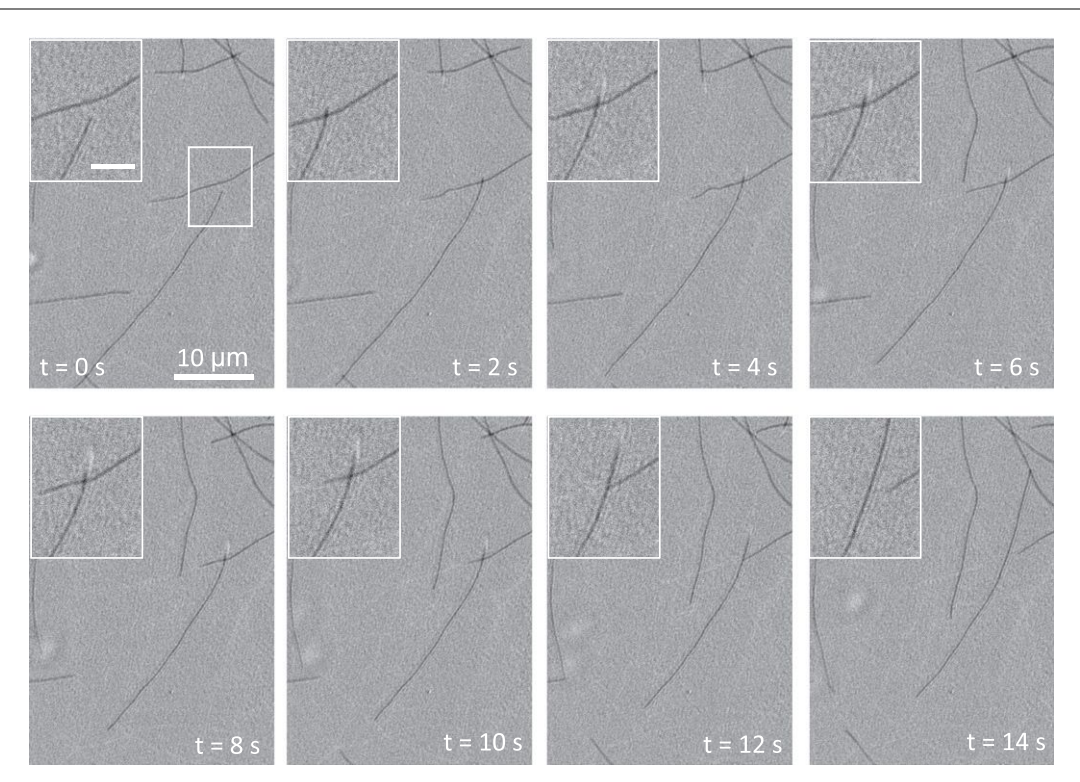


Figure 3. Time lapse images of a microtubule crossing over another microtubule. Inset shows the marked area, the meeting point, with scale bar: 3 μ m. The background has been subtracted using method 2 (background image is the median of 300 images).

illumination achieved via an off-center position of the aperture diaphragm were critical for visible contrast. To further reduce photodamage by removing blue and UV wavelengths, we added a 620 nm bandpass filter in the excitation filter position of the filter cube (see supplementary figure S1) (https://stacks.iop.org/NJP/ 22/095002/mmedia). In IRM (figure 1(b)), contrast is derived from the interference between the light reflected by the glass/liquid interface (not phase-shifted) and the light reflected by the liquid/microtubule interface (phase-shifted by half a wavelength). A microtubule near the surface will thus appear dark against a lighter background (figure 2(a)). As Mahamdeh et al pointed out, illumination irregularities and static noise also generate contrast but can be removed by background subtraction, with the background image being calculated by averaging a set of images before the observation window or taking a median of 100 images after the observation window while moving the stage. In our experiments, we observed microtubules gliding on surface-adhered kinesins over hours where the stage could drift several micrometers. We achieved slightly better background correction if we calculated the background image by calculating (1) either the median of 150 images from different locations before the observation begins (figure 2(b)), or (2) the median of many frames acquired during the observation window (figure 2(d)). To avoid negative numbers 25 counts were added to the images before subtracting the background. After background subtraction, high contrast images are obtained (figures 2(c) and (e) and supplementary movie S1). The first method (median of images from different locations) is not very good for longer measurements (>1 h), due to slight movements of the focus and the stage. An advantage is that immobile objects on the surface appear in the subtracted image. The second method (median of images in the observation window) is better for longer measurements because at any time the median over many images around that time frame is calculated (figure 2(d)). With this second method, immobile objects on the surface can be pinpointed in the background image (e.g. inset figure 2(d)) but can appear with halos in the subtracted image due to stage drift (figure 2(e)). We primarily used the second method because we were measuring for longer periods of time and were not specifically interested in the immobile objects on the surface.

3.2. IRM is used to follow a crossover event

The contrast in IRM images also yields information about the height of the imaged objects near the surface. Objects directly on or close to the surface or at a height of $m\lambda_{\text{water}}/2$, m=0,1,2,... will be dark (destructive interference) while objects that are at a height of $m\lambda_{\text{water}}/4$, m=1,3,5,... above the surface will appear bright (constructive interference). Similar to fluorescence interference contrast (FLIC) microscopy, calibration of the object intensity can yield nanometer resolution of the object height [26].

New J. Phys. 22 (2020) 095002 G Saper and H Hess

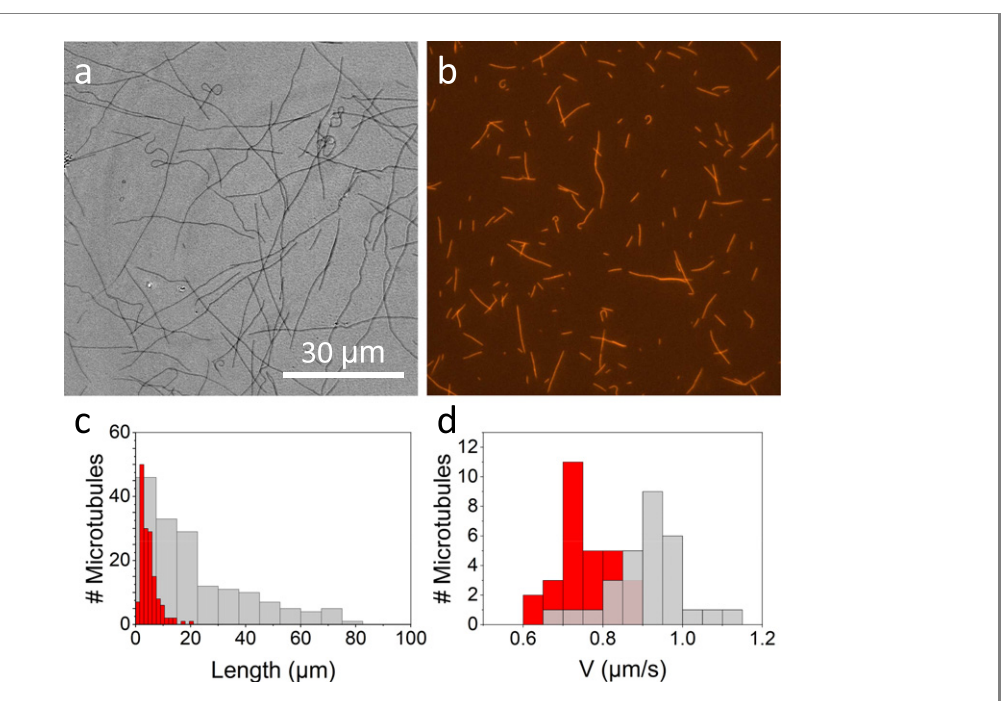


Figure 4. Label-free microtubules are longer and move faster than rhodamine-labeled microtubules. (a) IRM image of label-free microtubules. (b) Fluorescence microscopy image of rhodamine-labeled microtubules. (c) Histogram of the length of label-free (gray) and rhodamine-labeled (red) microtubules. (d) Histogram of the velocity of kinesin propelled label-free (gray) and rhodamine-labeled (red) microtubules imaged with IRM in the presence of the oxygen scavenger system (OSS).

Here, we merely illustrate this aspect by imaging microtubule crossover events [27], which occur when microtubules collide and one microtubule crosses over the other one. Some of these events lead to the crossing microtubule leaving the surface, while in most cases the crossing microtubule continues on its path [28]. Figure 3 shows such a crossover event: at time t=2 s (relative to the first frame) the microtubule moving upwards is crossing the microtubule moving to the right, and at t=4 s the tip of the microtubule moving upwards becomes bright, indicating detachment from the surface to a height of approximately 150 nm. Between 6 and 12 s the microtubule tip is not seen anymore (it must keep advancing as the tail continues to move), while the last visible segment of the microtubules remains bright indicating that it is elevated from the surface. At t=14 s the microtubule fully reattaches to the surface, with the tip reappearing in black 10 μ m away from the crossover location. This matches the simulations of microtubules crossing the edge of a kinesin track [29], and could explain why shorter microtubules leave the surface due to crossover events [28]. Note that our background subtraction method (median of images in the observation window) leaves the trajectories of the microtubules faintly visible as bright paths.

3.3. Label-free microtubules are longer, move at higher velocities and experience less photodamage compared to rhodamine-labelled microtubules.

Label-free microtubules imaged with IRM exhibit different lengths and gliding velocities compared to rhodamine-labelled microtubules also imaged with IRM. The average length of label-free microtubules was $21 \pm 2 \,\mu\mathrm{m}$ (mean \pm S.E.M.) while the average length of the rhodamine-labelled microtubules polymerized using the same protocol was only $4.7 \pm 0.3 \mu m$ (figures 4(a)-(c)), suggesting that the fluorophores interfere with microtubule assembly to a small degree as has been observed previously [30]. Both length distributions are consistent with the Schulz length distribution of in vitro polymerized microtubules described by Jeune-Smith et al [31]. The velocity of label-free microtubules was $0.91 \pm 0.02 \ \mu \text{m} \cdot \text{s}^{-1}$ (mean \pm S.E.M.) while the velocity of rhodamine-labeled microtubules was only $0.75 \pm 0.01 \ \mu \text{m} \cdot \text{s}^{-1}$ imaged with IRM (figures 4(d)) and $0.74 \pm 0.02 \ \mu \text{m} \cdot \text{s}^{-1}$ imaged with fluorescence microscopy (supplementary figure S2(a)). To confirm that the difference in velocity was not caused by the variance in length we plotted the velocity as a function of microtubule length and found no significant correlation (supplementary figure S2(b)). This suggests that the velocity difference between the label-free and rhodamine-labelled microtubules is caused by the rhodamine labels either constituting obstacles to kinesin stepping [16] or facilitating persistent attachment to the surface caused by light-induced reactions [32]. The second possibility is supported by the observation that rhodamine-labeled microtubules imaged with IRM get stuck earlier than label-free microtubules imaged with IRM (supplementary figure S3). This is further supported by measurements of rhodamine-labeled microtubules imaged with fluorescent microscopy without antifade that show that the

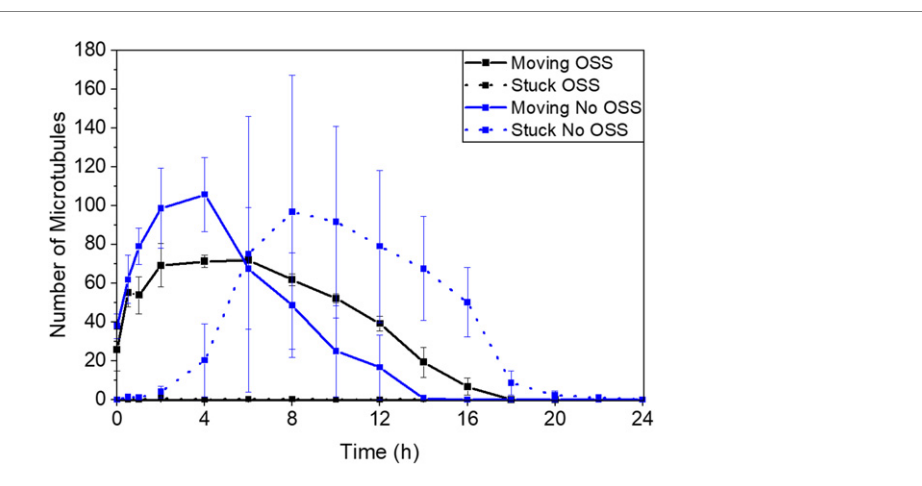


Figure 5. IRM is used to image the gliding assay without the OSS. The average number of microtubules in a field of view $(7876~\mu\text{m}^2)$ of three independent measurements as a function of time measured for the gliding assay. The gliding assay was conducted with label-free microtubules and imaged with IRM in the presence (black) or absence (blue) of the OSS. The full lines represent moving microtubules and the dashed lines stuck, non-moving, microtubules. The error bars are the standard error of the mean of three experiments.

microtubules get stuck immediately after the onset of illumination with excitation light (supplementary movie S2).

IRM permits long-term imaging of gliding microtubules, which usually struggles with photodamage caused by reactive oxygen species [13, 33], since it requires lower light intensities. In addition, the insertion of a filter transmitting only long wavelengths (590–650 nm) into the excitation filter position of the filter cube permits the selection of the lowest energy of the spectrum of the excitation light source. This further reduces the production of reactive oxygen species without reducing the signal-to-noise ratio despite the lower overall light intensity (see supplementary figure S1). We also compared the motility in gliding assays imaged with IRM with and without the enzymatic oxygen scavenging system (figure 5). While the number of moving microtubules decreases at a similar rate in both conditions (reduced to 50% after 10 h), microtubules do not get stuck in the presence of the scavenging system whereas in its absence 50% are stuck after 8 ± 2 h of continuous illumination (supplementary figure S4 and table S1). Thus IRM reduces but does not completely eliminate the photodamage associated with imaging. However, this method can be used in the future to measure the effect of oxygen radicals on kinesin propelled label-free microtubules.

4. Conclusions

IRM as described by Mahamdeh et al can not only image microtubules immobilized on the surface but also microtubules gliding on surface-adhered kinesins. IRM allows label-free imaging, and we found that microtubules polymerized from unlabeled tubulin are longer and move faster compared to rhodamine-labeled microtubules. In addition, IRM contrast is dependent on the height of the object above the surface, which can be helpful in interpreting dynamic events, such as the crossing of one gliding microtubule by another. Finally, photodamage due to imaging is reduced, especially if long wavelengths and an oxygen scavenging system are employed, but not eliminated. IRM can thereby play a valuable role for the design of kinesin/microtubule-based nanodevices with applications in actuating, sensing, signaling, and computing [34–38], e.g. by revealing the presence of non-fluorescent objects on the surface [28]. The presence of electrodes [39], guiding structures [40], and microtubule-bound cargo [41] in biomolecular motor-driven nanodevices may complicate IRM imaging, but also reveal important information which is complementary to the information gained from fluorescence imaging. Due to the smaller diameter of actin filaments and their larger distance from the surface when they are propelled by surface-adhered myosins [42], IRM may yield only low contrast images for actin/myosin-based assays and devices, which is a point for further exploration. Ultimately, IRM is less sensitive than FLIC imaging which precludes the imaging of individual molecular events, but shines when label-free imaging of nanostructures is required.

Author contributions

GS and HH designed the experiments and wrote the manuscript. GS conducted the measurements and analyzed the results.

Acknowledgments

Financial support under NSF Grant ENG 1662329 is gratefully acknowledged. This work was performed, in part, at the Center for Integrated Nanotechnologies, an Office of Science User Facility operated for the US Department of Energy (DOE) Office of Science by Los Alamos National Laboratory (contract DE-AC52-06NA25396) and Sandia National Laboratories (contract DE-AC04- 94AL85000).

ORCID iDs

Henry Hess https://orcid.org/0000-0002-5617-606X

References

- [1] Howard J 2001 Mechanics of Motor Proteins and the Cytoskeleton (Sunderland, MA: Sinauer Associates)
- [2] Saper G and Hess H 2019 Synthetic systems powered by biological molecular motors Chem. Rev. 120 288-309
- [3] Howard J, Hunt A J and Baek S 1993 Chapter 10 assay of microtubule movement driven by single kinesin molecules *Methods Cell Biol.* 39 137–47
- [4] Uppalapati M, Huang Y-M, Shastry S, Jackson T N and Hancock W O 2009 Microtubule motors in microfluidics *Methods in Bioengineering: Microfabrication and Microfluidics* ed J D Zahn and L P Lee (Boston, MA: Artech House) pp 311–37
- [5] Dong C and Dinu C Z 2013 Molecular trucks and complementary tracks for bionanotechnological applications *Curr. Opin. Biotechnol.* **24** 612–9
- [6] Keya J J et al 2018 Control of swarming of molecular robots Sci. Rep. 8 11756
- [7] Weiss D G, Langford G M, Seitz-Tutter D and Maile W 1991 Analysis of the gliding, fishtailing and circling motions of native microtubules *Acta Histochem Suppl* **41** 81–105
- [8] Spector J O, Vemu A and Roll-Mecak A 2020 In vitro microtubule dynamics assays using dark-field microscopy Cytoskeleton Dynamics (Berlin: Springer) pp 39–51
- [9] Kuriyama R and Miki-Noumura T 1975 Light-microscopic observations of individual microtubules reconstituted from brain tubulin J. Cell Sci. 19 607–20
- [10] Horio T and Hotani H 1986 Visualization of the dynamic instability of individual microtubules by dark-field microscopy Nature 321 605-7
- [11] Walker R A, O'Brien E T, Pryer N K, Soboeiro M F, Voter W A, Erickson H P and Salmon E D 1988 Dynamic instability of individual microtubules analyzed by video light microscopy: rate constants and transition frequencies *J. Cell Biol.* 107 1437–48
- [12] Bieling P, Telley I A, Hentrich C, Piehler J and Surrey T 2010 Fluorescence microscopy assays on chemically functionalized surfaces for quantitative imaging of microtubule, motor, and+ TIP dynamics *Methods in Cell Biology* vol 95 (Amsterdam: Elsevier) pp 555–80
- [13] Vigers GP, Coue M and McIntosh JR 1988 Fluorescent Microtubules break up under illumination J. Cell Biol. 107 1011-24
- [14] Yan P, Xiong Y, Chen B, Negash S, Squier T C and Mayer M U 2006 Fluorophore-assisted light inactivation of calmodulin involves singlet-oxygen mediated cross-linking and methionine oxidation *Biochemistry* 45 4736–48
- [15] Brunner C, Ernst K-H, Hess H and Vogel V 2004 Lifetime of biomolecules in polymer-based hybrid nanodevices Nanotechnology 15 S540
- [16] Korten T and Diez S 2008 Setting up roadblocks for kinesin-1: mechanism for the selective speed control of cargo carrying microtubules Lab Chip 8 1441-7
- [17] Bormuth V, Howard J and Schäffer E 2007 LED illumination for video-enhanced DIC imaging of single microtubules *J. Microsc.*
- [18] Gutiérrez-Medina B and Block S M 2010 Visualizing individual microtubules by bright field microscopy Am. J. Phys. 78 1152-9
- [19] Kandel M E, Teng K W, Selvin P R and Popescu G 2017 Label-free imaging of single microtubule dynamics using spatial light interference microscopy ACS Nano 11 647–55
- [20] Mahamdeh M, Simmert S, Luchniak A, Schäffer E and Howard J 2018 Label-free high-speed wide-field imaging of single microtubules using interference reflection microscopy J. Microsc. 272 60–6
- [21] Koch M D and Rohrbach A 2018 Label-free imaging and bending analysis of microtubules by ROCS microscopy and optical trapping Biophys. J. 114 168–77
- [22] Simmert S, Abdosamadi M K, Hermsdorf G and Schäffer E 2018 LED-based interference-reflection microscopy combined with optical tweezers for quantitative three-dimensional microtubule imaging Opt. Express 26 14499–513
- [23] Andrecka J, Arroyo J O, Lewis K, Cross R A and Kukura P 2016 Label-free imaging of microtubules with sub-nm precision using interferometric scattering microscopy *Biophys. J.* 110 214–7
- [24] Coy D L, Wagenbach M and Howard J 1999 Kinesin takes one 8-nm step for each ATP that it hydrolyzes J. Biol. Chem. 274 3667–71
- [25] Mahamdeh M and Howard J 2019 Implementation of interference reflection microscopy for label-free, high-speed imaging of microtubules J. Vis. Exp. 150 e59520
- [26] Kerssemakers J, Howard J, Hess H and Diez S 2006 The distance that kinesin holds its cargo from the microtubule surface measured by fluorescence-interference-contrast microscopy Proc. Natl Acad. Sci. 103 15812-7
- [27] Boal A K, Bachand G D, Rivera S B and Bunker B C 2006 Interactions between cargo-carrying biomolecular shuttles Nanotechnology 17 349–54
- [28] Bassir Kazeruni N M, Rodriguez J, Saper G and Hess H 2020 Microtubule detachment in gliding motility assays limits the performance of kinesin-driven molecular shuttles *Langmuir* 36 7901–7
- [29] Ishigure Y and Nitta T 2014 Understanding the guiding of kinesin/microtubule-based microtransporters in microfabricated tracks Langmuir 30 12089–96
- [30] Howard J and Hyman A A 1993 Preparation of marked microtubules for the assay of the polarity of microtubule-based motors by fluorescence microscopy *Methods in Cell Biology* vol 39 (Amsterdam: Elsevier) pp 105–13

New J. Phys. 22 (2020) 095002 G Saper and H Hess

[31] Jeune-Smith Y and Hess H 2010 Engineering the length distribution of microtubules polymerized in vitro Soft Matter 6 1778-84

- [32] Surrey T, Elowitz M B, Wolf P-E, Yang F, Nedelec F, Shokat K and Leibler S 1998 Chromophore-assisted light inactivation and self-organization of microtubules and motors *Proc. Natl Acad. Sci.* 95 4293–8
- [33] Kabir A M R, Inoue D, Kakugo A, Kamei A and Gong J P 2011 Prolongation of the active lifetime of a biomolecular motor for *in vitro* motility assay by using an inert atmosphere *Langmuir* 27 13659–68
- [34] Chaudhuri S, Korten T, Korten S, Milani G, Lana T, te Kronnie G and Diez S 2017 Label-free detection of microvesicles and proteins by the bundling of gliding microtubules Nano Lett. 18 117–23
- [35] Nicolau D V et al 2016 Parallel computation with molecular-motor-propelled agents in nanofabricated networks Proc. Natl Acad. Sci. USA 113 2591–6
- [36] Keya J J et al 2018 DNA-assisted swarm control in a biomolecular motor system Nat. Commun. 9 453
- [37] Fischer T, Agarwal A and Hess H 2009 A smart dust biosensor powered by kinesin motors Nature Nanotech 4 162-6
- [38] Aoyama S, Shimoike M and Hiratsuka Y 2013 Self-organized optical device driven by motor proteins *Proc. Natl Acad. Sci.* 110 16408–13
- [39] Ramsey L *et al* 2014 Control and gating of kinesin-microtubule motility on electrically heated thermo-chips *Biomed. Microdevices* **16** 459–63
- [40] Hiratsuka Y, Tada T, Oiwa K, Kanayama T and Uyeda T Q P 2001 Controlling the direction of kinesin-driven microtubule movements along microlithographic tracks *Biophys. J.* 81 1555–61
- [41] Nitzsche B, Ruhnow F and Diez S 2008 Quantum-dot-assisted characterization of microtubule rotations during cargo transport Nat. Nanotechnol. 3 552–6
- [42] Persson M, Albet-Torres N, Ionov L, Sundberg M, Höök F, Diez S, Månsson A and Balaz M 2010 Heavy meromyosin molecules extending more than 50 nm above adsorbing electronegative surfaces *Langmuir* 26 9927–36